Specifying and Sustaining Pigmentation Patterns in Domestic and Wild Cats

Christopher B. Kaelin *et al.*

Science **337**, 1536 (2012);
DOI: 10.1126/science.1220893

tion involves a large displacement of H1, stabilized by new salt bridges with β-tubulin, and an opening of CC1 at the base of the stalk (Fig. 4E). The movements of H1 and CC1 likely constrain the registries that can be explored by the stalk, biasing the distribution toward the high-affinity α registry (Fig. 4E). Propagation of this signal to the head would elicit conformational changes that produce a movement of the linker domain and a displacement of dynein toward the MT minus end.

Our analysis of dynamic salt bridges reveals that cytoplasmic dynein has been selected for submaximal processivity. Whereas kinesin has diversified its functional repertoire through gene duplication and divergence (*33*), cytoplasmic dynein is expressed from a single locus and may have evolved suboptimal processivity to increase the dynamic range of its regulation. High processivity could also be detrimental when multiple dyneins and kinesins must balance their actions on a single cargo (*34*). Consistent with this idea, intraflagellar dyneins, responsible for long, unidirectional transport within cilia (*35*, *36*), contain neutral or basic residues at the equivalent of H6-E3378 (fig. S12), which would likely increase their processivity.

References and Notes

1. I. R. Gibbons, *Cell Motil. Cytoskeleton* **32**, 136 (1995).
2. P. Höök, R. B. Vallee, *J. Cell Sci.* **119**, 4369 (2006).
3. R. D. Vale, *Cell* **112**, 467 (2003).
4. R. B. Vallee, G. E. Seale, J.-W. Tsai, *Trends Cell Biol.* **19**, 347 (2009).
5. R. B. Vallee, J. C. Williams, D. Varma, L. E. Barnhart, *J. Neurobiol.* **58**, 189 (2004).
6. S. A. Burgess, M. L. Walker, H. Sakakibara, P. J. Knight, K. Oiwa, *Nature* **421**, 715 (2003).
7. A. J. Roberts *et al.*, *Cell* **136**, 485 (2009).
8. I. R. Gibbons, B. H. Gibbons, G. Mocz, D. J. Asai, *Nature* **352**, 640 (1991).
9. T. Kon, M. Nishiura, R. Ohkura, Y. Y. Toyoshima, K. Sutoh, *Biochemistry* **43**, 11266 (2004).
10. S. L. Reck-Peterson, R. D. Vale, *Proc. Natl. Acad. Sci. U.S.A.* **101**, 1491 (2004).
11. S. L. Reck-Peterson *et al.*, *Cell* **126**, 335 (2006).
12. T. Shima, T. Kon, K. Imamula, R. Ohkura, K. Sutoh, *Proc. Natl. Acad. Sci. U.S.A.* **103**, 17736 (2006).
13. A. P. Carter, C. Cho, L. Jin, R. D. Vale, *Science* **331**, 1159 (2011).
14. T. Kon, K. Sutoh, G. Kurisu, *Nat. Struct. Mol. Biol.* **18**, 638 (2011).
15. M. P. Koonce, *J. Biol. Chem.* **272**, 19714 (1997).
16. M. A. Gee, J. E. Heuser, R. B. Vallee, *Nature* **390**, 636 (1997).
17. A. P. Carter *et al.*, *Science* **322**, 1691 (2008).
18. I. R. Gibbons *et al.*, *J. Biol. Chem.* **280**, 23960 (2005).
19. T. Kon *et al.*, *Nat. Struct. Mol. Biol.* **16**, 325 (2009).
20. T. Kon *et al.*, *Nature* **484**, 345 (2012).
21. N. Mizuno *et al.*, *EMBO J.* **23**, 2459 (2004).
22. C. V. Sindelar, K. H. Downing, *J. Cell Biol.* **177**, 377 (2007).
23. C. V. Sindelar, K. H. Downing, *Proc. Natl. Acad. Sci. U.S.A.* **107**, 4111 (2010).
24. D. B. Wells, A. Aksimentiev, *Biophys. J.* **99**, 629 (2010).
25. J. Löwe, H. Li, K. H. Downing, E. Nogales, *J. Mol. Biol.* **313**, 1045 (2001).
26. L. G. Trabuco, E. Villa, K. Mitra, J. Frank, K. Schulten, *Structure* **16**, 673 (2008).
27. L. G. Trabuco, E. Villa, E. Schreiner, C. B. Harrison, K. Schulten, *Methods* **49**, 174 (2009).
28. J. Schlitter, M. Engels, P. Krüger, *J. Mol. Graph.* **12**, 84 (1994).
29. S. Uchimura, Y. Oguchi, Y. Hachikubo, S. Ishiwata, E. Muto, *EMBO J.* **29**, 1167 (2010).
30. M. P. Koonce, I. Tikhonenko, *Mol. Biol. Cell* **11**, 523 (2000).
31. Z. Wang, M. P. Sheetz, *Biophys. J.* **78**, 1955 (2000).
32. L. McNaughton, I. Tikhonenko, N. K. Banavali, D. M. LeMaster, M. P. Koonce, *J. Biol. Chem.* **285**, 15994 (2010).
33. E. M. Dagenbach, S. A. Endow, *J. Cell Sci.* **117**, 3 (2004).
34. M. A. Welte, *Curr. Biol.* **14**, R525 (2004).
35. C. Iomini, V. Babaev-Khaimov, M. Sassaroli, G. Piperno, *J. Cell Biol.* **153**, 13 (2001).
36. J. A. Laib, J. A. Marin, R. A. Bloodgood, W. H. Guilford, *Proc. Natl. Acad. Sci. U.S.A.* **106**, 3190 (2009).

Acknowledgments: We thank A. Carter (Laboratory of Molecular Biology-Medical Research Council) for reagents and advice, C. Sindelar (Yale), V. Ramey [University of California (UC)–Berkeley], E. Egelman (University of Virginia), and R. Sinkovits (UC–San Diego) for sharing processing scripts and helpful advice; M. Sotomayor (Harvard) and R. Gaudet (Harvard) for advice concerning MD; J. Hogle (Harvard), M. Strauss (Harvard), and M. Wolf (Harvard) for help with film and the use of a film scanner; and E. Nogales (UC-Berkeley), N. Francis (Harvard), and D. Pellman (Harvard) for critically reading the manuscript, as well as all the members of the Leschziner and Reck-Peterson Labs for advice and helpful discussions. EM data were collected at the Center for Nanoscale Systems (CNS), a member of the National Nanotechnology Infrastructure Network (NNIN), which is supported by the National Science Foundation under NSF award no. ECS-0335765. CNS is part of Harvard University. MD simulations were run on the Odyssey cluster supported by the Faculty of Arts and Sciences Science Division Research Computing Group, Harvard University. S.L.R.-P. is funded by the Rita Allen Foundation, the Harvard Armenise Foundation, and an NIH New Innovator award (1 DP2 OD004268-1). A.E.L. was funded in part by a Research Fellowship from the Alfred P. Sloan Foundation. R.H.-L. was supported in part by Consejo Nacional de Ciencia y Tecnología and Fundación México en Harvard. The cryo-EM map was deposited at the EM Data Bank (EMDB-5439) and pseudo-atomic models at the Protein Data Bank (PDB-3J1T and -3J1U).

Supplementary Materials

www.sciencemag.org/cgi/content/full/337/6101/1532/DC1
Materials and Methods
Figs. S1 to S12
Tables S1 to S3
References (*37*–*53*)
Movies S1 to S6

2 May 2012; accepted 20 July 2012
10.1126/science.1224151

Specifying and Sustaining Pigmentation Patterns in Domestic and Wild Cats

Christopher B. Kaelin,[1,2]* Xiao Xu,[3,4]* Lewis Z. Hong,[2] Victor A. David,[3] Kelly A. McGowan,[2] Anne Schmidt-Küntzel,[3,5] Melody E. Roelke,[3,6] Javier Pino,[7] Joan Pontius,[3,6] Gregory M. Cooper,[1] Hermogenes Manuel,[2] William F. Swanson,[8] Laurie Marker,[5] Cindy K. Harper,[9] Ann van Dyk,[10] Bisong Yue,[4] James C. Mullikin,[11] Wesley C. Warren,[12] Eduardo Eizirik,[13,14] Lidia Kos,[7] Stephen J. O'Brien,[3]†‡ Gregory S. Barsh,[1,2]† Marilyn Menotti-Raymond[3]

Color markings among felid species display both a remarkable diversity and a common underlying periodicity. A similar range of patterns in domestic cats suggests a conserved mechanism whose appearance can be altered by selection. We identified the gene responsible for tabby pattern variation in domestic cats as *Transmembrane aminopeptidase Q* (*Taqpep*), which encodes a membrane-bound metalloprotease. Analyzing 31 other felid species, we identified *Taqpep* as the cause of the rare king cheetah phenotype, in which spots coalesce into blotches and stripes. Histologic, genomic expression, and transgenic mouse studies indicate that paracrine expression of *Endothelin3* (*Edn3*) coordinates localized color differences. We propose a two-stage model in which *Taqpep* helps to establish a periodic pre-pattern during skin development that is later implemented by differential expression of *Edn3*.

The molecular basis and evolutionary variation of periodic mammalian color patterns have been difficult to investigate from genetic crosses of model organisms. Domestic cats (*Felis catus*) exhibit heritable variation of tabby markings—mackerel versus blotched—that provide an opportunity for such genetic analysis (*1*). Tabby markings are a composite of two features: (i) a light background component in which individual hairs have extensive light bands, and (ii) a superimposed darker component in which hairs have little or no banding. In mackerel cats, the dark component is organized into narrow vertical stripes with a constant and regular spacing, whereas in blotched cats, the dark component is expanded into a less organized structure with wide whorls (Fig. 1A). Periodic color patterns in other felids may represent the same process; for example, dark tabby markings in domestic cats may be homologous to black stripes or spots in tigers or cheetahs, respectively (*2*).

A logical explanation for tabby patterning involves the Agouti-melanocortin receptor system, in which Agouti protein, a paracrine signaling molecule released from dermal papillae, acts on overlying hair follicle melanocytes to inhibit the melanocortin 1 receptor (Mc1r), causing a switch from the production of black/brown eumelanin to red/yellow pheomelanin (*3*, *4*). According to this hypothesis, dark tabby stripes are areas in which Agouti signaling is suppressed or surmounted during hair growth and regeneration. However, known components of the Agouti-melanocortin

pathway do not affect the shape of tabby patterns (*1*, *2*, *5*, *6*). Instead, the difference between mackerel and blotched is controlled by a single locus, *Tabby* (*Ta*), whose genetic position does not suggest an obvious candidate gene (*7*) but whose effects could be manifested via differential control of melanocortin signaling.

The 3X cat genome assembly is not contiguous across the *Tabby* linkage interval (*7*), but comparison to homologous regions in the dog and human genomes suggests a candidate interval of ~5 Mb in length (fig. S1A). Old World wild cats, from which domestic cats arose ~10,000 years ago (*8*), exhibit a mackerel-like pattern. However, the blotched pattern is common in many modern breeds, suggesting that one or a few Ta^b causal variants would lie in a region of reduced allelic variation due to recent selection. We used comparative genomic information to identify single-nucleotide polymorphisms (SNPs) in the candidate interval, then genotyped and analyzed 16 blotched (Ta^b/Ta^b) and 33 mackerel (Ta^M/Ta^M or Ta^M/Ta^b) animals from a feral population in northern California. Five SNPs from a 180-kb interval on chrA1 showed significant association (P range = 9×10^{-4} to 3.2×10^{-9}) (fig. S1B).

Twenty-four markers genotyped in and around the associated region in 58 blotched and 19 mackerel cats indicated that all blotched animals shared a common haplotype extending for 244 kb, whereas mackerel samples exhibited several haplotypes within the same interval (figs. S1C and S2). Coding sequences from three genes are located within the 244-kb interval: *Commd10*, *LOC644100*, and a third gene whose human ortholog has been referred to as both *Aminopeptidase Q* and *Laeverin* (*9*). No sequence alterations were observed in *LOC644100* or *Commd10*, but most blotched cats carried a nonsense mutation, W841X (Fig. 1B, fig. S2, and table S1), in exon 17 of the third gene. We subsequently identified two additional variants in the same gene, S59X and D228N (Fig. 1B, fig. S2, and table S1). This gene is expressed in developing felid skin, and its loss of function causes a loss of color pattern periodicity

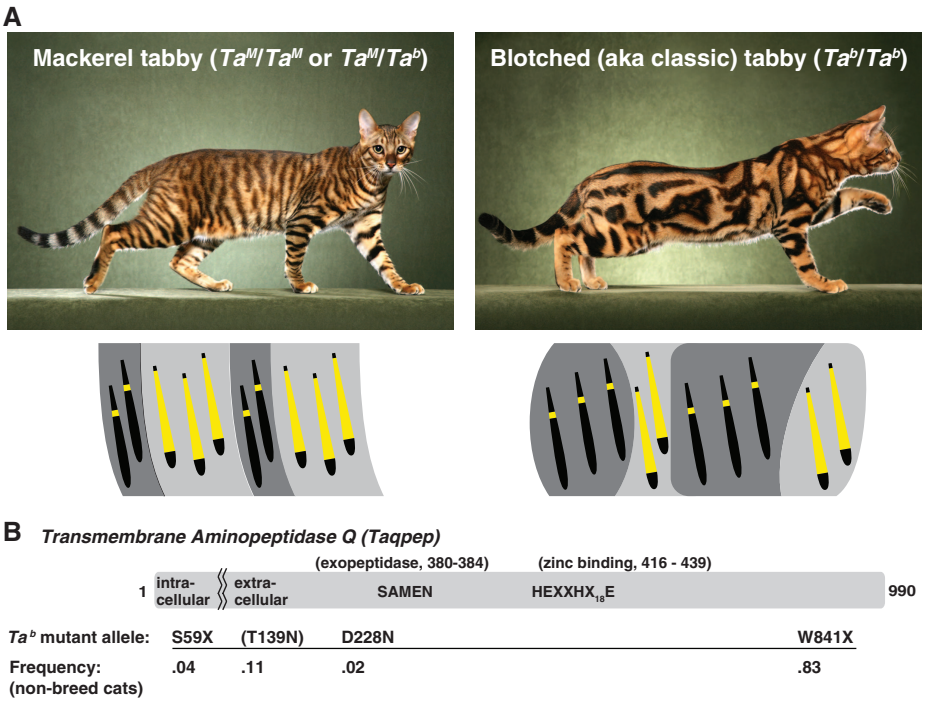

Fig. 1. (A) Allelic variation at *Tabby* [mackerel (Ta^M) is dominant to blotched (Ta^b)] controls the arrangement of dark- and light-colored areas. Diagrams indicate how the distribution of black or brown eumelanin versus yellow or pale pheomelanin within individual hairs underlies the macroscopic color patterns, although in reality cat hairs frequently exhibit multiple pheomelanic bands. (**B**) *Taqpep* encodes a type II membrane protein with aminopeptidase activity encoded by the ectodomain. Mutant allele frequencies are from a survey of 119 feral and outbred cats (table S1). The T139N allele is associated (P = 0.0017, Fisher's exact test) with an atypical swirled pattern but is incompletely penetrant (table S1 and fig. S2).

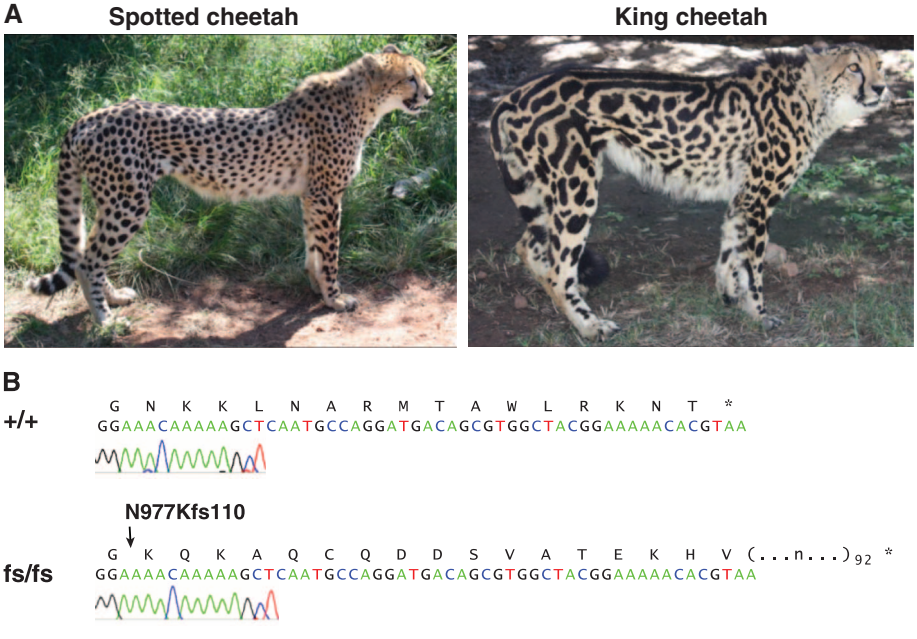

Fig. 2. (**A**) Black-haired areas are larger, more irregular, and associated with dorsal stripes in the king cheetah. (**B**) Chromatogram of *Taqpep* cDNA from a spotted (+/+) as compared to a king (fs/fs) cheetah.

[1]HudsonAlpha Institute for Biotechnology, Huntsville, AL 35806, USA. [2]Department of Genetics, Stanford University, Stanford, CA, 94305, USA. [3]Laboratory of Genomic Diversity, Frederick National Laboratory for Cancer Research, Frederick, MD 21702, USA. [4]Sichuan Key Laboratory of Conservation Biology on Endangered Wildlife, College of Life Sciences, Sichuan University, Sichuan 610064, China. [5]Cheetah Conservation Fund, Post Office Box 1755, Otjiwarongo, Namibia. [6]SAIC-Frederick, Frederick National Laboratory for Cancer Research, Frederick, MD 21702, USA. [7]Department of Biological Sciences, Florida International University, Miami, FL 33199, USA. [8]Center for Conservation and Research of Endangered Wildlife, Cincinnati Zoo & Botanical Garden, Cincinnati, OH 45220, USA. [9]Veterinary Genetics Laboratory, Faculty of Veterinary Science Onderstepoort, University of Pretoria, Pretoria, South Africa. [10]The Ann van Dyk Cheetah Centre, De Wildt, South Africa. [11]Comparative Genomics Unit, National Human Genome Research Institute, National Institutes of Health, Rockville, MD 20892, USA. [12]The Genome Center, Washington University in St. Louis, St. Louis, MO 63108, USA. [13]Faculdade de Biociências, Pontifícia Universidade Católica do Rio Grande do Sul, Porto Alegre, Rio Grande do Sul 90619-900, Brazil. [14]Instituto Pró-Carnívoros, Atibaia, Brazil.

*These authors contributed equally to this work.
†To whom correspondence and requests for materials should be addressed. E-mail: gbarsh@hudsonalpha.org (G.S.B.); lgdchief@gmail.com (S.J.O'B.).
‡Present address: Theodosius Dobzhansky Center for Genome Informatics, St. Petersburg State University, St. Petersburg, Russia.

without obvious effects on other organ systems. We refer to this gene as *Transmembrane Aminopeptidase Q* (*Taqpep*) and the protein product as Tabulin to reflect its organismal function.

Taqpep encodes a type II membrane-spanning protein of the M1 aminopeptidase family, whose members are characterized by the presence of GAMEN exopeptidase (SAMEN in Taqpep) and $HEXXHX_{18}E$ zinc-binding motifs in their extracellular domains (Fig. 1B) (*9*). In feral cats, we observed homozygosity or compound heterozygosity for the Ta^b S59X or W841X alleles in 58 out of 58 (58/58) blotched animals, with no phenotypic distinction among the different genotypic classes, compared to 51/51 mackerel cats that carried 0 or 1 Ta^b alleles (table S1). A third Ta^b allele, D228N, was found to cosegregate with the blotched phenotype in a research colony (fig. S2D). In feral cats, we also observed two variants at codon 139, one of which, T139N, was significantly associated (P = 0.0017, Fisher's exact test) with an atypical swirled pattern (figs. S2 and S4D and table S1) and therefore may represent hypomorphic or neomorphic activity. Overall, the mutant W841X allele predominates and is responsible for the strong haplotype signature (fig. S1C), although the S59X allele occurs on the same haplotype background, in trans to W841X (fig. S2).

Cheetahs (*Acinonyx jubatus*) with the rare king pattern were originally described as a distinct felid species (*10*) but were later recognized as having a monogenic trait with an autosomal recessive mode of inheritance (*11*). In king cheetahs, the black spots coalesce into larger areas, and multiple longitudinal black stripes appear on the dorsum (Fig. 2A). Wild king cheetahs have been sighted only in a small area of sub-Saharan Africa (fig. S3) (*11*). *Taqpep* genomic sequence from a captive king cheetah in North America revealed a base pair insertion in exon 20, predicting a frameshift that replaces what would normally be the carboxy-terminal 16 amino acids with 109 new residues (N977Kfs110, Fig. 2B). Additional DNA samples from captive cheetahs in a large pedigree demonstrated complete cosegregation of the king pattern with the N977Kfs110 mutation [LOD (logarithm of odds) score = 5.7], and further revealed that the mutant allele was introduced into the pedigree by one homozygous and two heterozygous animals (fig. S3). We did not detect the N977Kfs110 mutation in wild cheetahs caught in Namibia (n = 191), Tanzania (n = 23), or Kenya (n = 3).

Depictions of tabby markings from the Middle Ages are mostly mackerel, but the blotched phenotype increased to a sufficiently high frequency to be described by Linnaeus in 1758 as characteristic for the domestic cat, predating the formation of most modern breeds. We examined the predicted Tabulin sequence in 351 cats from 24 breeds (table S2) and observed that the W841X allele is polymorphic in most breeds of Western origin, but rare or absent in Eastern breeds. The high allele frequency for W841X in Abyssinian (1.0), Birman (0.71), and Himalayan (0.77) cats is especially notable, because tabby markings in these breeds are masked by epistatic interactions. The S59X allele, probably representing a complete ablation of protein function, is most common in Norwegian Forest Cats, and we observed one S59X/S59X homozygote with a blotched phenotype.

We determined *Taqpep* sequence for 31 wild felid species, identifying 130 synonymous and 64 nonsynonymous predicted substitutions (fig. S4A). We assessed the potential functional impact of the nonsynonymous substitutions with multivariate analysis of protein polymorphism (MAPP) (*12*), a quantitative approach that takes into account both evolutionary conservation and side-chain physicochemical properties. A MAPP score >10 indicates a likely impact on protein function, and the T139N and D228N substitutions associated with atypical swirled and blotched mutant phenotypes, respectively, in the domestic cat yield MAPP scores of 11 ($P = 1.5 \times 10^{-3}$) and 14 ($P = 3.9 \times 10^{-4}$) (fig. S4B). In contrast, the T139A variant in the domestic cat (which does not affect pattern) yields a MAPP score of 3.8. The black-footed cat (*Felis nigripes*) is a clear outlier from other Felidae, with five lineage-specific nonsynonymous substitutions and a combined MAPP score of 50 (fig. S4C). *F. nigripes* exhibits a spotting phenotype that is similar to the atypical swirled pattern associated with the T139N allele in domestic cats (fig. S4D); thus, recent evolution of *Taqpep* in *F. nigripes* may contribute to its characteristic pattern.

To investigate how color patterns are implemented, we examined fetal cat skin at 3, 5, and 7 weeks of gestation, and observed that the first histologic indication of tabby markings coincides with their external appearance at 7 weeks, when follicle architecture is established and hair shafts begin to protrude through the epidermal surface

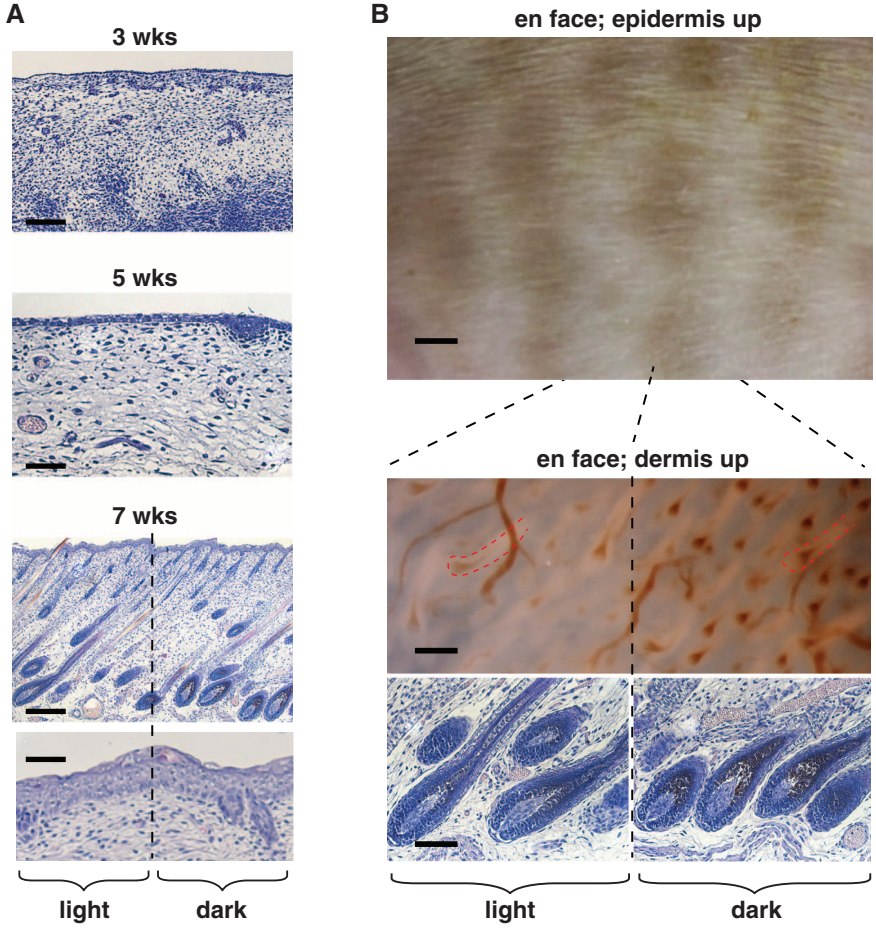

Fig. 3. Skin sections of fetal cats [(**A**), at 3, 5, and 7 weeks of gestation] stained with hematoxylin and eosin, together with unstained flat-mount (en face) skin preparations of fetal cats [(**B**), at 7 weeks of gestation]. The 7-week images in (B) are from an orange (*O/Y* or *O/O*) individual, which allows the dark component of the tabby pattern (which is orange-colored) to be more easily visualized. In the trans-illuminated "dermis-up" panel, hair follicle outlines (dashed red lines) appear light-colored; melanin incorporation and blood vessels appear dark-colored. Scale bars in (A), 150, 50, and 250 μm in 3-, 5-, and 7-week fetal cat sections, respectively, and 50 μm in the 7-week epidermis close-up. Scale bars in (B), 2 mm, 100 μm, and 600 μm in epidermis-up, follicle histology, and dermis-up panels, respectively.

(Fig. 3). At this stage, the boundary between dark and light tabby components reflects differences in the amount of melanin deposition, with no apparent difference in cell type; melanocytes are present in both dark and light areas but produce more melanin in dark areas. Furthermore, the density and architecture of hair follicles are independent of localization to dark and light areas (Fig. 3B). This suggests that tabby markings arise from spatial variation in transcriptional activity rather than cell type distribution.

We used the EDGE (EcoP15I-tagged Digital Gene Expression) (*13*) method for gene expression profiling to examine the transcriptome of cheetah skin, in which there are sharp boundaries between black spots and the yellow interspot areas and for which multiple skin biopsies were available for study. Cheetah skin exhibits an unusual histologic architecture; the epidermis is heavily pigmented, and hair follicles are organized in clusters with extensive accessory structures (Fig. 4A and fig. S5A). However, the number and size of follicle clusters, as well as the number of epidermal pigment cells, do not vary between black-haired and yellow-haired areas (fig. S5B). Based on a previous analysis of EDGE results from a single cheetah, we hypothesized that black coloration involves localized alterations of genes downstream of Mc1r signaling (*13*). Biopsies of yellow- and black-colored areas from five different animals enabled a genome-wide approach, in which the expression of 14,014 genes could be measured across a 10^6-fold dynamic range (Fig. 4B). At a false discovery rate (q) < 0.05, we identified 74 differentially expressed genes (tables S7 and S8).

Among 60 genes up-regulated in black as compared to yellow cheetah skin, 7 are melanocyte-specific, of which 4 [*Tyr* (4.9-fold, $q = 3.8 \times 10^{-19}$), *Silv* (7.3-fold, $q = 1 \times 10^{-36}$), *Dct* (3.2-fold, $q = 5.3 \times 10^{-8}$), and *Tyrp1* (3.1-fold, $q = 1.7 \times 10^{-5}$)] encode pigment type-switching components (*14*, *15*). Genes that encode ligands or regulators of Mc1r signaling are not differentially expressed between yellow and black cheetah skin (Fig. 4B and table S7). However, one of the nonmelanocytic genes up-regulated in black as compared to yellow cheetah skin (4.9-fold, $q = 2.1 \times 10^{-4}$), *Edn3*, a paracrine hormone expressed mostly by mesenchymal cells that promotes differentiation and proliferation of melanocytes and other neural

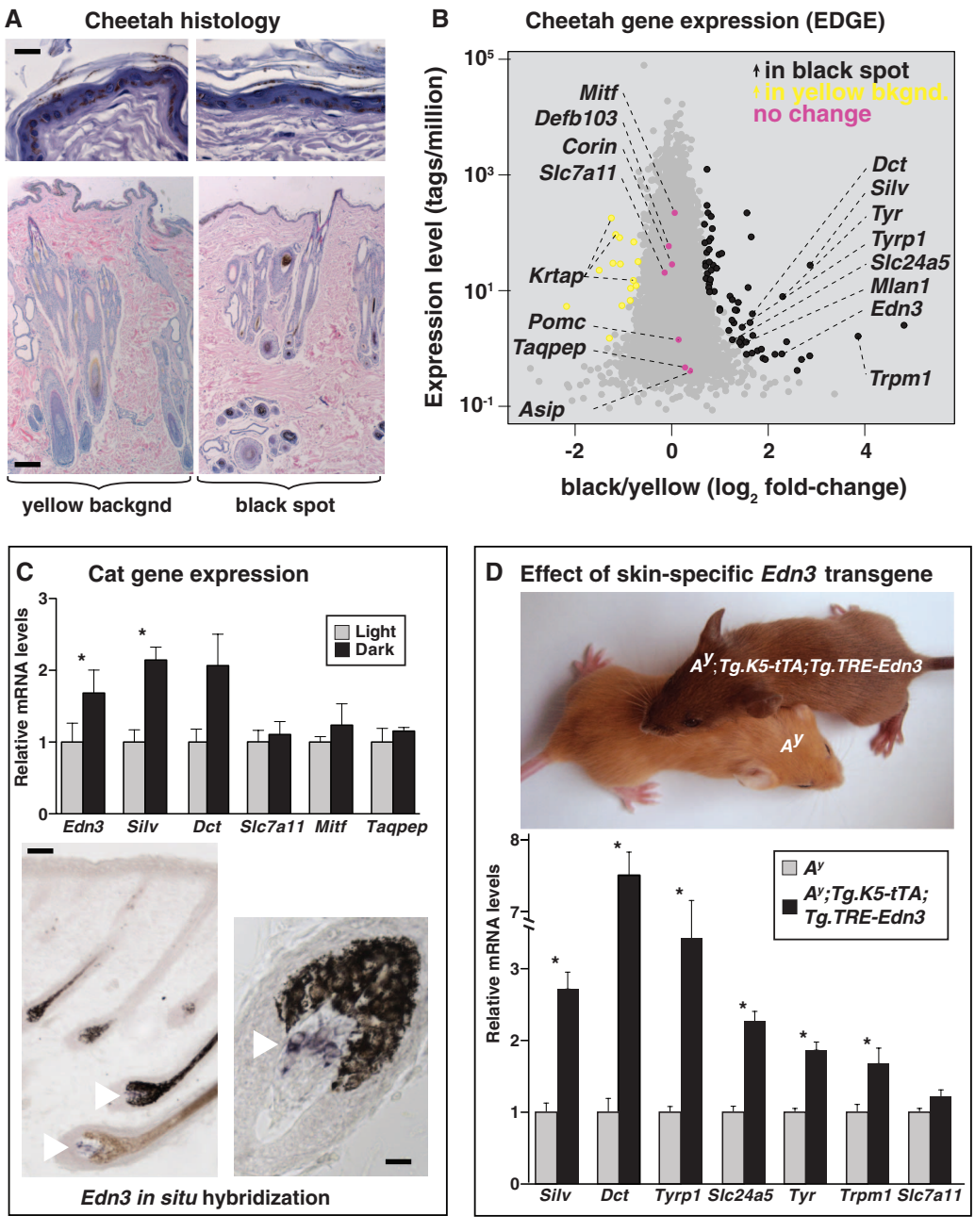

Fig. 4. (**A**) A cheetah skin biopsy that includes a black-yellow boundary (also see fig. S6). (**B**) EDGE (*13*) determination of differential gene expression in black- as compared to yellow-colored areas of cheetah skin. Transcript frequency (observations per million sequence reads, mean of five samples) is plotted as a function of differential expression. The 74 genes with significant differential expression are shown in black or yellow (FDR < 0.05, see methods and tables S8 and S9); 7 additional pigmentation genes that are not differentially expressed are shown in pink. (**C**) Relative mRNA levels (mean ± SE) for the indicated genes as assessed by qRT-PCR from paired samples ($n = 4$) of dark and light neonatal tabby skin; *$P < 0.05$ (dark versus light, two-tailed t test). Dermal papilla expression of *Edn3* mRNA (purple stain, white arrows) as detected by in situ hybridization, from a brown tabby individual. The left panel illustrates the expression of *Edn3* mRNA in both pheomelanin- and eumelanin-containing follicles. (**D**) Phenotypes of 2-week-old mice of the indicated genotypes. Relative mRNA levels (mean ± SE) for the indicated genes from qRT-PCR of cDNA from control ($n = 4$) and transgenic ($n = 4$) mice are shown; *$P < 0.05$ (A^y versus A^y;*Tg.K5-tTA;Tg.TRE-Edn3*, two-tailed t test). Scale bars in (A), 40 and 200 μm in epidermis and whole-skin sections, respectively. In (C), 60 and 20 μm in left and right panels, respectively.

crest derivatives, is a candidate for the coordination of spatial variation in hair color. A hypermorphic mutation of Gnaq, the second messenger through which Edn3 acts, causes the accumulation of dermal melanocytes during embryogenesis and converts yellow hair to black in postnatal mice (*16*, *17*).

Quantitative reverse transcription polymerase chain reaction (qRT-PCR) confirmed that the expression of *Edn3* and *Silv* was increased in black-colored as compared to yellow-colored areas of cheetah skin; we also observed similar increases in a single leopard skin sample (fig. S5C). In neonatal skin from domestic cats (in which there is a high proportion of anagen follicles), *Edn3* mRNA expression was also ~twofold higher in dark as compared to light areas (Fig. 4C), and in situ hybridization revealed that expression was restricted to the dermal papilla, a permanent portion of the hair follicle.

In A^y mutant mice, which express high levels of Agouti protein and produce pheomelanin instead of eumelanin, we confirmed that an *Edn3* transgene (*18*) converts yellow hair to dark brown–colored hair (Fig. 4D). Using qRT-PCR, we observed that the *Edn3* transgene in mice also caused increased expression of the same melanocyte-specific genes that are overexpressed in black-colored areas of cheetah skin (Fig. 4B). Thus, increased expression of *Edn3* in transgenic mice probably recapitulates both the coat color and melanocytic gene expression phenotypes observed in cheetah skin, which suggests that localized expression of *Edn3* during felid hair follicle growth serves as a master regulator of spatial hair color differences associated with tabby markings.

In the skin of neonatal domestic cats and adult cheetahs, *Taqpep* mRNA is expressed at low levels that do not differ between dark and light areas (Fig. 4, B and C). In mice, levels of whole-embryo *Taqpep* mRNA as measured by qRT-PCR increased progressively during gestation and were highest in postnatal skin (fig. S6). In situ hybridization to mouse embryos (at embryonic days 10.5 to 17.5) and to fetal cat skin at 3, 5, 6, and 7 weeks of gestation did not reveal localization of *Taqpep* mRNA to any specific cell type or region.

Because tabby markings are apparent soon after the time when melanocytes enter hair follicles (Fig. 3A), the effects of *Taqpep* on pattern morphology must occur at or before follicle development and are therefore likely to be mediated by epithelial or mesenchymal cells. Our results suggest that *Taqpep* is required to establish the periodicity of tabby markings during skin development (Fig. 5A), and that the "tabby marking" identity of a particular region is implemented and maintained by the ability of dermal papilla cells to sustain high versus low levels of *Edn3* production throughout subsequent hair cycles (Fig. 5B). This model also helps to explain why, in contrast to many periodic color patterns in fish, which are mediated by and depend on direct contact between pigment cells (*19*–*21*), tabby markings change in size but not number during organismal growth.

Our findings also provide a mechanistic explanation for epistasis relationships between *Agouti*, *Mc1r*, and *Tabby*. Homozygosity for a loss-of-function *Agouti* allele is associated with a "ghost pattern" in which Tabby stripes are difficult or impossible to visualize, because eumelanogenic genes such as *Tyr*, *Tyrp1*, *Dct*, and *Pmel* are already upregulated. The ghost pattern becomes apparent, however, in animals that are doubly mutant for *Agouti* and *Mc1r* (*5*), because endothelin and melanocortin signaling act in parallel (fig. S7). A system in which distinct paracrine signaling pathways—endothelins via a $G\alpha_q$-coupled receptor and melanocortins via a $G\alpha_s$-coupled receptor—converge on overlapping cellular machinery could explain more complicated phenotypes, in which pheomelanin-rich yellow versus eumelanin-rich black areas exhibit both periodic and regional fluctuation, such as spots or stripes of alternative pigment types overlaid on a background of dorsoventral differences, as is apparent in leopards, jaguars, and tigers. Further studies of color pattern in domestic-wild cat hybrids offer the opportunity to study these complex color markings and add to our knowledge of how felids acquire their color patterns.

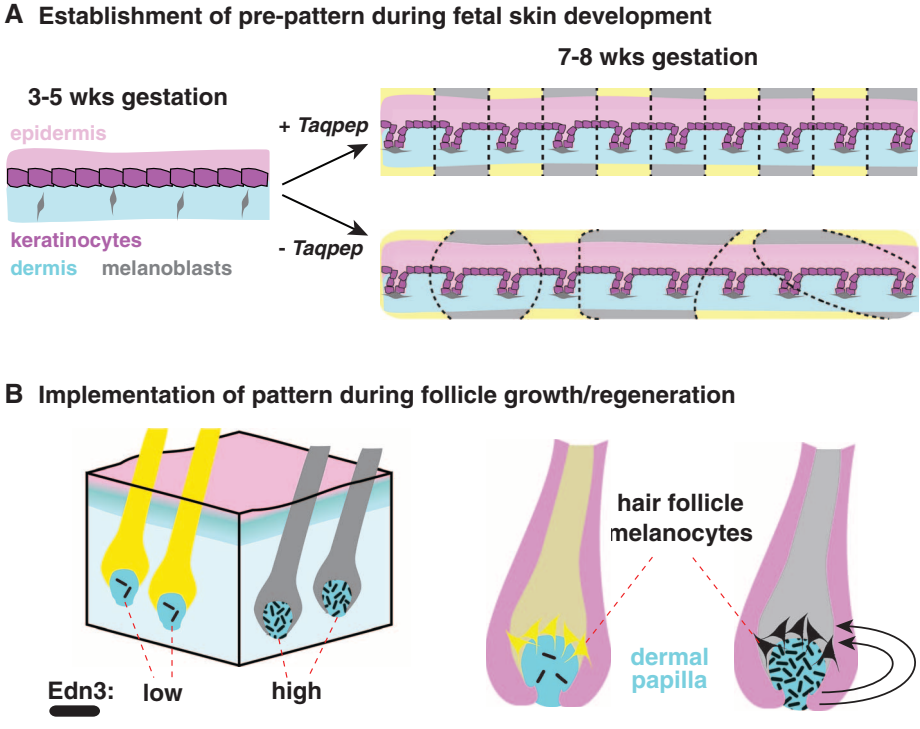

Fig. 5. A tabby pre-pattern is established at or before hair follicle development (**A**), specifying regions as dark (gray-colored) or light (yellow-colored). In the absence of *Taqpep*, dark regions are expanded, and there is less periodicity. Regional identity is manifested and implemented (**B**) by differential expression of *Edn3* in the dermal papilla, a permanent part of the hair follicle that releases paracrine factors to act on overlying melanocytes. Yellow and black pigment are synthesized by melanocytes in hair follicles that produce low and high levels of *Edn3*, respectively.

References and Notes

1. T. D. Lomax, R. Robinson, *J. Hered.* **79**, 21 (1988).
2. A. G. Searle, *Comparative Genetics of Coat Color in Mammals* (Academic Press, New York, 1968).
3. S. E. Millar, M. W. Miller, M. E. Stevens, G. S. Barsh, *Development* **121**, 3223 (1995).
4. I. J. Jackson, *Annu. Rev. Genet.* **28**, 189 (1994).
5. M. Peterschmitt, F. Grain, B. Arnaud, G. Deléage, V. Lambert, *Anim. Genet.* **40**, 547 (2009).
6. E. Eizirik *et al.*, *Curr. Biol.* **13**, 448 (2003).
7. E. Eizirik *et al.*, *Genetics* **184**, 267 (2010).
8. C. A. Driscoll *et al.*, *Science* **317**, 519 (2007).
9. M. Maruyama *et al.*, *J. Biol. Chem.* **282**, 20088 (2007).
10. R. I. Pocock, *Proc. Zool. Soc. London* **97**, 245 (1927).
11. R. J. van Aarde, A. van Dyk, *J. Zool.* **209**, 573 (1986).
12. E. A. Stone, A. Sidow, *Genome Res.* **15**, 978 (2005).
13. L. Z. Hong, J. Li, A. Schmidt-Küntzel, W. C. Warren, G. S. Barsh, *Genome Res.* **21**, 1905 (2011).
14. C. S. April, G. S. Barsh, *Pigment Cell Res.* **19**, 194 (2006).
15. T. Kobayashi *et al.*, *J. Cell Sci.* **108**, 2301 (1995).
16. C. D. Van Raamsdonk, K. R. Fitch, H. Fuchs, M. H. de Angelis, G. S. Barsh, *Nat. Genet.* **36**, 961 (2004).
17. C. D. Van Raamsdonk, G. S. Barsh, K. Wakamatsu, S. Ito, *Pigment Cell Melanoma Res.* **22**, 819 (2009).
18. R. J. Garcia *et al.*, *J. Invest. Dermatol.* **128**, 131 (2008).
19. A. Nakamasu, G. Takahashi, A. Kanbe, S. Kondo, *Proc. Natl. Acad. Sci. U.S.A.* **106**, 8429 (2009).
20. M. Iwashita *et al.*, *PLoS Genet.* **2**, e197 (2006).
21. M. Watanabe *et al.*, *EMBO Rep.* **7**, 893 (2006).

Acknowledgments: We thank San Jose Animal Care and Services, Fix Our Ferals, the Berkeley East-Bay Humane Society, Pets In Need, the Monterey Animal Hospital, and the City of Huntsville Animal Shelter for assistance with sample collection; the Wild Cat Education and Conservation Fund for contributing king cheetah samples; R. Finn for assistance with Norwegian Forest Cat samples and phenotypes; H. Flick for domestic cat photographs; and J. C. Kaelin for help with feral cat sample collection. We thank the Production Sequencing Group of the Washington University School of Medicine Genome Center for cDNA sequencing. Namibian samples were collected with the approval of the Ministry of Environment and Tourism (permit

1532). Supported in part by the HudsonAlpha Institute for Biotechnology and by the Intramural Research Program of the NIH, National Cancer Institute, Center for Cancer Research, using federal funds under contract N01-CO-12400. L.Z.H. and J.P. were supported by fellowships from Genentech and the National Institutes of Health, respectively. A.vD. is the founder and director of the Ann van Dyk Cheetah Centre, a nonprofit conservation organization. DNA sequence data for this study are available at http://genome.wustl.edu/genomes/view/felis_catus/ and the NIH Short Read Archive (SRA056885).

Supplementary Materials
www.sciencemag.org/cgi/content/full/337/6101/1536/DC1
Materials and Methods
Supplementary Text
Tables S1 to S9
Figs. S1 to S7
References (*22*–*36*)

22 February 2012; accepted 20 July 2012
10.1126/science.1220893

Loss of the Tumor Suppressor BAP1 Causes Myeloid Transformation

Anwesha Dey,[1] Dhaya Seshasayee,[2] Rajkumar Noubade,[2] Dorothy M. French,[3] Jinfeng Liu,[4] Mira S. Chaurushiya,[1] Donald S. Kirkpatrick,[5] Victoria C. Pham,[5] Jennie R. Lill,[5] Corey E. Bakalarski,[4] Jiansheng Wu,[5] Lilian Phu,[5] Paula Katavolos,[6] Lindsay M. LaFave,[7] Omar Abdel-Wahab,[7] Zora Modrusan,[8] Somasekar Seshagiri,[8] Ken Dong,[9] Zhonghua Lin,[10] Mercedesz Balazs,[10] Rowena Suriben,[1] Kim Newton,[1] Sarah Hymowitz,[9] Guillermo Garcia-Manero,[11] Flavius Martin,[2] Ross L. Levine,[7] Vishva M. Dixit[1]*

De-ubiquitinating enzyme BAP1 is mutated in a hereditary cancer syndrome with increased risk of mesothelioma and uveal melanoma. Somatic *BAP1* mutations occur in various malignancies. We show that mouse *Bap1* gene deletion is lethal during embryogenesis, but systemic or hematopoietic-restricted deletion in adults recapitulates features of human myelodysplastic syndrome (MDS). Knockin mice expressing BAP1 with a 3xFlag tag revealed that BAP1 interacts with host cell factor–1 (HCF-1), O-linked *N*-acetylglucosamine transferase (OGT), and the polycomb group proteins ASXL1 and ASXL2 in vivo. OGT and HCF-1 levels were decreased by *Bap1* deletion, indicating a critical role for BAP1 in stabilizing these epigenetic regulators. Human *ASXL1* is mutated frequently in chronic myelomonocytic leukemia (CMML) so an ASXL/BAP1 complex may suppress CMML. A *BAP1* catalytic mutation found in a MDS patient implies that BAP1 loss of function has similar consequences in mice and humans.

Somatic inactivating *BAP1* mutations occur in the majority of metastatic uveal melanomas and approximately one-quarter of malignant pleural mesotheliomas. Somatic mutations also have been identified in breast, lung, and renal cell cancers (*1*–*5*). Recently, germline *BAP1* mutations were linked to a tumor predisposition syndrome characterized by melanocytic tumors, mesothelioma, and uveal melanoma (*6*, *7*).

We investigated the normal physiological role of BAP1 using BAP1-deficient mice (fig. S1A). $Bap1^{-/-}$ embryos showed developmental retardation at embryonic day 8.5 (E8.5) and were not detected beyond E9.5, indicating that BAP1 is essential for embryo development (fig. S1, B and C). To bypass this embryonic lethality, we bred mice that expressed the tamoxifen-inducible recombinase creERT2 ubiquitously from the *Rosa26* locus (*8*) and had *Bap1* exons 4 and 5 flanked by lox sites (floxed) (fig. S1A). The floxed *Bap1* exons were deleted from most adult mouse tissues at 1 week after daily tamoxifen injections for 5 days were completed, the brain being the expected exception (fig. S1D). Loss of *Bap1* mRNA from hematopoietic lineages at 1 week after the final tamoxifen injection was confirmed by quantitative reverse transcription polymerase chain reaction (fig. S1E), and BAP1 protein was no longer detected in splenocytes by Western blotting (fig. S1F). Within 4 weeks of the last tamoxifen injection, 100% of the $Bap1^{fl/fl}$ creERT2^{+} mice [hereafter referred to as BAP1 knockout (BAP1 KO) mice] developed splenomegaly (n = 12 mice). This phenotype was never observed in $Bap1^{+/+}$ creERT2^{+} control mice [hereafter referred to as wild-type (WT) mice] (Fig. 1, A and B). Histopathology, flow cytometry, and myeloperoxidase immunohistochemistry revealed that splenomegaly in the KO mice resulted from extramedullary hematopoiesis and expansion of the myeloid lineage (Fig. 1, C to E). Myeloid cells also were increased in lymph nodes (fig. S2) and bone marrow (Fig. 1F).

Peripheral blood taken from 11 out of 12 BAP1 KO mice at 4 weeks after the final tamoxifen injection showed cytological features consistent with myelodysplasia and ineffective erythropoiesis (Fig. 1G). Total leukocyte numbers were elevated (Fig. 1H) because of monocytosis (Fig. 1I) and neutrophilia (Fig. 1J), which is consistent with chronic myelomonocytic leukemia (CMML)–like disease [classified as a myelodysplastic/myeloproliferative disease according to the new World Health Organization classification of myeloid neoplasms (*9*)]. Thrombocytopenia was detected as early as 1 week after the final tamoxifen injection (Fig. 1K), and all diseased mice developed severe progressive anemia (Fig. 1L). We noted morphologic features of erythroid dysplasia, including increased numbers of nucleated red blood cells, anisopoikilocytosis, and prominent basophilic stippling (Fig. 1L). Hypersegmented neutrophils (Fig. 1J), bilobed granulocytes (Fig. 1I), giant platelets (Fig. 1K), hyposegmented neutrophils consistent with pseudo-Pelger-Huët anomaly, and atypical immature cells with myelomonocytic features were also observed. Mitotic figures and apoptotic cells (fig. S3) were consistent with human myelodysplastic syndrome (MDS) (*10*), whereas blasts were rare. Collectively, these data show that *Bap1* deletion produces a myeloproliferative/myelodysplastic disorder with features of human CMML. Consistent with what is seen in patients with end-organ damage from myeloid neoplasms, the BAP1 KO heart contained microthrombi with multifocal necrosis, neutrophilic inflammation, and infiltration of myeloblastic cells (fig. S4).

Given that chronic myeloid neoplasms originate in the phenotypic hematopoietic stem cell (HSC) compartment (*11*), we characterized the lineage-depleted hematopoietic progenitor cell population in the BAP1 KO mice. Lineage-negative ScaI^{-} c-Kit^{+} myeloid progenitor cells and HSC-enriched lineage-negative ScaI^{+} c-Kit^{+} (LSK) cells were increased in BAP1 KO spleen and bone marrow as early as 2 weeks after the final tamoxifen injection (fig. S5A). Given that BAP1 KO mice develop monocytosis and neutrophilia, BAP1 KO LSK cells harvested 1 month after tamoxifen treatment expressed higher levels of a subset of genes involved in myelopoiesis [fig. S5, B and C (*12*)]. In methylcellulose colony-forming assays, BAP1 KO LSK cells yielded fewer colonies than WT LSK cells (fig. S6, A and B). In addition, unlike cells from WT colonies, which could be replated after 10 days in culture to form new colonies, replated BAP1 KO cells did not produce well-formed colonies, and many exhibited cytoplasmic blebbing characteristic of apoptosis (fig. S6, C and D). These in vitro data suggest that BAP1

[1]Department of Physiological Chemistry, Genentech, 1 DNA Way, South San Francisco, CA 94080, USA. [2]Department of Immunology, Genentech, 1 DNA Way, South San Francisco, CA 94080, USA. [3]Department of Pathology, Genentech, 1 DNA Way, South San Francisco, CA 94080, USA. [4]Department of Bioinformatics and Computational Biology, Genentech, 1 DNA Way, South San Francisco, CA 94080, USA. [5]Department of Protein Chemistry, Genentech, 1 DNA Way, South San Francisco, CA 94080, USA. [6]Department of Safety Assessment, Genentech, 1 DNA Way, South San Francisco, CA 94080, USA. [7]Human Oncology and Pathogenesis Program and Leukemia Service, Memorial Sloan-Kettering Cancer Center, 1275 York Avenue, New York, NY 10065, USA. [8]Department of Molecular Biology, Genentech, 1 DNA Way, South San Francisco, CA 94080, USA. [9]Department of Structural Biology, Genentech, 1 DNA Way, South San Francisco, CA 94080, USA. [10]Department of Translational Immunology, Genentech, 1 DNA Way, South San Francisco, CA 94080, USA. [11]MD Anderson Cancer Center, 1515 Holcombe Boulevard, Houston, TX 77030, USA.

*To whom correspondence should be addressed. E-mail: dixit@gene.com